Bull. Mater. Sci., Vol. 36, No. 4, August 2013, pp. 699–708. © Indian Academy of Sciences.

Rietveld analysis, dielectric and impedance behaviour of Mn^{3+}/Fe^{3+} ion-modified $Pb(Zr_{0.65}Ti_{0.35})O_3$ perovskite

NIRANJAN SAHU* **and S PANIGRAHI**
Department of Physics, National Institute of Technology, Rourkela 769 008, India

MS received 3 June 2011; revised 29 August 2012

Abstract. **The polycrystalline samples of $Pb(Zr_{0.65-x}A_xTi_{0.35})O_3$ (A = Mn/Fe), (x = 0·00, 0·05) (PZM/FT) were synthesized by conventional solid-state reaction technique. X-ray diffraction (XRD) pattern was recorded at room temperature and the samples were found in single phase form. All the observed peaks could be indexed to *R3c* space group with rhombohedral symmetry. XRD pattern has been analysed by employing Rietveld method with the help of FullProf Program. The lattice parameters and unit cell volumes decrease from Mn^{3+} to Fe^{3+} ion concentrations. The bond lengths and angles have been calculated by using Powder Cell Programme. Microstructural analysis of the surface of the ceramic compound by scanning electron microscopy (SEM) exhibits that there is a significant change in grain size on introduction of Mn^{3+} and Fe^{3+} ions at the Zr-site of the compound. It is observed that both the substitutions (Mn^{3+} and Fe^{3+}) at Zr site induce an increase in dielectric constant and a shift in Curie temperature (T_c). From a.c. conductivity analysis, we have estimated the activation energy for both ferroelectric and paraelectric regions. Both the modified samples are obeying Jonscher power law. From Nyquist plots, the activation energy of grain resistance, relaxation time and bulk conductivity are compared. The grain resistance of the material decreases with rise in temperature which indicates a semiconducting behaviour of the material.**

Keywords. **Ceramics; X-ray diffraction; crystal structure; dielectric properties; electrical conductivity; Nyquist plots.**

1. Introduction

Pb-based ceramic oxides have been widely studied due to its excellent ferroelectric, dielectric and piezoelectric properties. In particular, $PbTiO_3$-based solid solutions have dominated the technological field for decades, responsible for the development of piezoelectric materials. Lead zirconium titanate belongs to the perovskite structural family with a general formula, ABO_3, in which A-site is occupied by Pb^{2+} ions and B-site by Zr^{4+} and/or Ti^{4+} ions (Klung and Alexander 1974; Lines and Glass 1977; Dorr 2006). The fluctuation of the oxidation state of Mn^{3+}/Fe^{3+} ions result in the formation of oxygen ion vacancies to reserve the local electrical neutrality and causes thermally activated conduction. Lead zirconium titanate (PZT) is a solid solution of ferroelectric $PbTiO_3$ (PT with T_c = 490 °C) and antiferroelectric $PbZrO_3$ (PZ with T_c = 230 °C) with different Zr/Ti ratios, has two ferroelectric phases: a tetragonal phase in the titanium rich side of the binary system and rhombohedral phase in the zirconium rich side (Xu *et al* 2006; Maiti *et al* 2007; Thakur *et al* 2009). The boundary line between these two phases is called morphotropic phase boundary (MPB) at which dielectric and conductive properties rise to a great extent (Rukmini *et al* 2000; Saha and Sinha 2006). A wide variety of complex compounds (other than the above) can be prepared by substituting suitable elements at the A and B sites of PZT, useful for different industrial applications such as dynamic and versatile memory components, capacitors, transducers, sensors, light-liquid crystal display, backlight inverters for camcorder, etc (Dimza 1996; Saha and Krupanidhi 2000; Majumder *et al* 2001; Boucher *et al* 2002; Dutta *et al* 2004). The selection of substituents to tailor physical properties of the material is based on many factors, i.e. charge neutrality, tolerance factor, ionic radius, solubility, etc. Magnetic materials (Mn^{3+} and Fe^{3+}) have been widely used as doping elements for the manufacture of multilayer ceramic capacitors (Jaffe *et al* 1971; Jin and Kim 1997; Tanasoiu *et al* 1999; Pandey *et al* 2009).

Recently, Tiwari and Choudhary (2008) showed the substitution of Mn and Ce on Zr site and improvement of dielectric constant and shift in T_c. It is observed that substitution of Mn (in small amounts) at Zr-site of PZT does not provide any change in its structure (Tiwari and Choudhary 2009a, b; Niranjan Sahu *et al* 2012), but Mn^{3+}/Fe^{3+} ions doping changes the particle density on the surface. Detailed literature survey reveals that not much work has been done on low doping of both Mn^{3+} and Fe^{3+} ions modified PZT ceramics (Herbert 1985; Wilkinson *et al* 1994; Dai *et al* 1995). However, electrical properties and frequency response at different temperatures of both the ion-modified PZT and related materials have hardly been reported in the literature (Härdtl and Hennings 1972; Haertling 1991; Rangaraju and Choudhary 2004). The ratio of Zr/Ti(65/35) forms a part of our study,

*Author for correspondence (nsahu76@gmail.com and nsahunitrkl@ gmail.com)

which includes ratios at and around MPB (Rukmini 1998; Ang *et al* 2000; Behera *et al* 2007). Most of the reported works have used Zr/Ti ratios different from ours and none have used both the ions as single dopants separately with crystallographic comparisons using three different (Scherrer and Rietveld) methods. Recently, Niranjan Sahu *et al* (2011) studied the estimation of crystallite size of PZT by taking above three different methods and also observed that the ferroelectric transition temperature decreases with the crystallite size. Again Niranjan Sahu and Panigrahi (2012) studied that the Al^{3+} ion is replacing Ti^{4+} ion on $PbTiO_3$ and from Rietveld refinement, it is observed that the goodness of fit parameters, bond lengths and angles are useful for the development of the perovskite structure of the materials. Keeping in view of these facts, we have carried out detailed studies of the Rietveld structural and microparameter analysis, microstructure, dielectric and impedance properties of Mn^{3+} and Fe^{3+} ion- modified PZT (Zr/Ti = 65/35) prepared by conventional solid-state reaction route. XRD method is a general technique to find out microparameter of the materials, otherwise another technique is needed to refine data from XRD data (Yogaraksa *et al* 2004). This method is used for accurate data. In this paper, Rietveld analysis is used to refine structure and microparameter of Mn^{3+}/Fe^{3+} substitution on B-site of PZT material. The complex impedance spectroscopy (CIS) is a powerful technique to evaluate the electrical behaviour (Jonscher 1983). Nyquist plots between imaginary part of the impedance ($-Z''$) on y-axis and the real part (Z') on x-axis lead to succession of semicircular arcs corresponding to each relaxation process. Semicircular or depressed circular arcs may be obtained depending on the number of processes involved with different time constants. A polycrystalline material usually contains grain, grain boundary and electrode contribution leading to three successive semicircles (Macdonald 1987). CIS technique has been used to analyse the electrical properties of several ferroelectric materials.

2. Experimental

Perovskite type $Pb(Zr_{0.65-x}A_xTi_{0.35})O_3$ ($A = Mn^{3+}/Fe^{3+}$) ($x = 0.00, 0.05$) (PZM/FT) ceramic have been prepared by solid-state method. Stoichiometric ratio of PbO (Loba Chemie, Mumbai), ZrO_2 (Loba Chemie, Mumbai), MnO_2 (E Merck India Ltd), Fe_2O_3 (E Merck India Ltd) and TiO_2 (E Merck India Ltd) with 99·9% purity were weighed by using a high precision electronic balance (Avon, Gr 202). The above materials were mixed thoroughly with the help of agate mortar and pestle. The grinding was carried out under acetone till acetone evaporated from the mortar. The mixture was ball milled for 8 h and pre-sintered at different temperatures with intermediate grindings. The final pre-sintered temperature was 900 °C for 12 h. The pre-sintered powders of the above compounds were pressed into cylindrical pellets of 6 mm diameter and 1 mm thickness under an uniaxial pressure of 6 ton using a hydraulic press. Polyvinyl alcohol (PVA) was used as the binder to prepare pellets. Finally, the pellets were sintered at 1100 °C for over 4 h in an alumina crucible. All the above sintering processes were carried out in air. The bulk densities of the sintered samples were measured by Archimedes method using distilled water as medium and found to be 97–98% of the theoretical density. XRD pattern at room temperature for the sample was recorded by using Philips PANalytical X'pert-MPD X-ray diffractometer (XRD) (Model-PW3020). CuKα radiation was used as X-ray source. The machine was operated at 35 kV and 30 mA in a wide range of Bragg angles 2θ ($20° \leq 2\theta \leq 80°$). The data was collected with step size of 0·02° and time constant of 1 s. Scanning electron micrograph was recorded using JEOL SEM (JEOL T-330) at room temperature. The pellets are made with high-purity silver paint electrodes on the flat polished surfaces and heated at 150 °C for 4 h to take dielectric and electrical measurements. The dielectric (capacitance and dissipation) and impedance parameters (phase angle) were obtained at an a.c. input signal level of 1·5 V at a wide temperature (40–500 °C) and frequency (100 Hz–100 kHz) ranges using a computer-controlled LCR HiTESTER/impedance analyser (HIOKI 3522-50) which is also attached with high temperature microwave furnace (Model: DPI-1200).

3. Results and discussion

3.1 *Rietveld structural and microparameter analysis*

Figure 1 compares X-ray diffraction patterns of powders calcined at temperature 900 °C for 12 h of $Pb(Zr_{0.65-x}A_xTi_{0.35})O_3$ ($A = Mn^{3+}/Fe^{3+}$) ($x = 0.00, 0.05$). X-ray diffraction patterns indicate that the sample is in single phase form. Figure 2 compares X-ray diffraction patterns

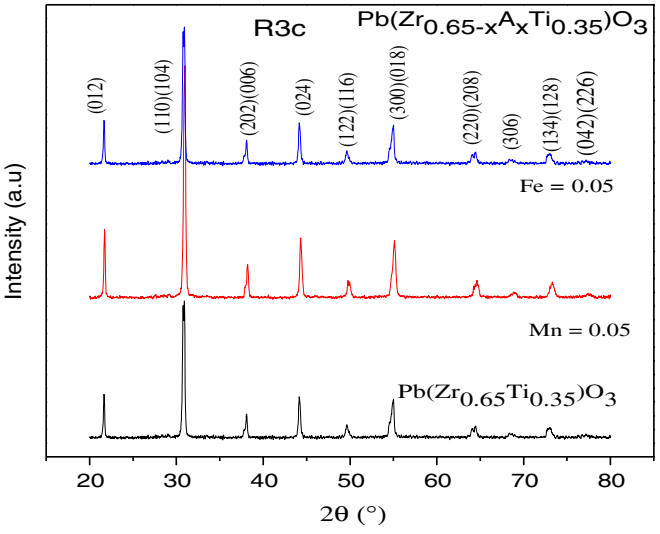

Figure 1. XRD patterns for samples $Pb(Zr_{0.65}Ti_{0.35})O_3$, $Pb(Zr_{0.60}Mn_{0.05}Ti_{0.35})O_3$ and $Pb(Zr_{0.60}Fe_{0.05}Ti_{0.35})O_3$ annealed at 900 °C for about 12 h.

of the samples sintered at 1100 °C for 4 h were found to be very sharp with distinct single diffraction peaks indicating good homogeneity and crystallization of the samples. The pattern clearly shows that there is no structural change of $Pb(Zr_{0\cdot65-x}A_xTi_{0\cdot35})O_3$ ($A = Mn^{3+}, Fe^{3+}$) ($x = 0\cdot00, 0\cdot05$) on substitution of small amount of Mn^{3+}/Fe^{3+} ion at Zr-site. It is observed that the structure is perovskite phase without any secondary phase, indicating complete diffusion of Mn^{3+}/Fe^{3+} ion into PZT lattice to form a single-phase compound. The unit cell parameters of rhombohedral system were refined using Rietveld refinement technique by employing Fullprof Program. The bond lengths and angles have been calculated with the help of Powder Cell Programme. The comparison of the crystallite size by using Scherrer's formulae, Williamson–Hall plot and Rietveld method have been estimated. Scherrer's formula is written as (Taylor 1961)

$$S_c = \kappa\lambda/\beta\cos\theta, \tag{1}$$

where constant 'κ' depends on the shape of the crystallite size (= 0·89, assuming the circular grain), β the full width at half maximum (FWHM) of intensity vs 2θ profile, λ the wavelength of CuKα radiation (0·15418 nm) and θ the Bragg's diffraction angle. The instrumental broadening factor has been taken into account during FWHM calculation $\left(\beta = \sqrt{\beta_{obs}^2 - \beta_{ins}^3}\right)$. The average crystallite values are listed in table 1 for both 900 °C and 1100 °C annealed samples. One can notice that average crystallite size increases with annealing temperature. It is due to the formation of larger crystals at high temperature, tolerance factor, ionic radii and solubility of the material.

According to Williamson–Hall (WH) (1953) method, individual contributions to the broadening of reflections can be expressed as

$$\beta\cos\theta = \frac{k\lambda}{S_c} + 4e\sin\theta, \tag{2}$$

where $4e\sin\theta$ is the strain effect on the crystallites. It is mostly the correction of Scherrer's formula by taking into account the strain. 2θ range of 20–80° were used to construct a linear plot of $\beta\cos\theta$ vs $\sin\theta$ (figure not shown), from which average crystallite size and strain were obtained using the above equation (WH). A complete expression is used in Rietveld method, which is written as (Young 1996)

$$\mathrm{FWHM}^2 = (U + D_{ST}^2)(\tan^2\theta) + V(\tan\theta) + W + \frac{IG}{\cos^2\theta}, \tag{3}$$

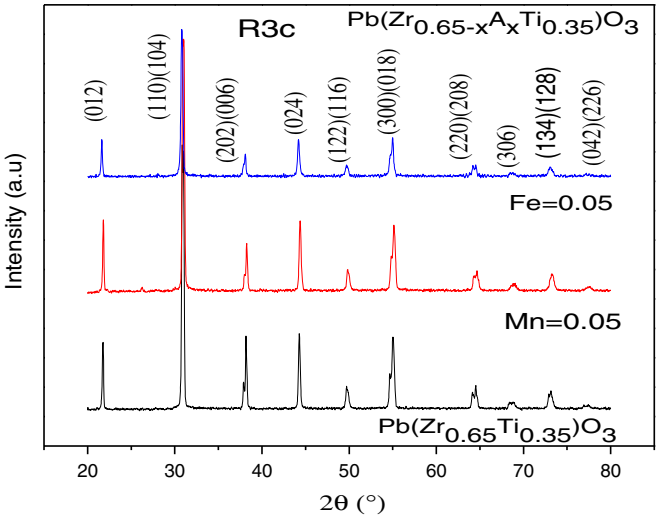

Figure 2. XRD patterns for samples $Pb(Zr_{0\cdot65}Ti_{0\cdot35})O_3$, $Pb(Zr_{0\cdot60}Mn_{0\cdot05}Ti_{0\cdot35})O_3$ and $Pb(Zr_{0\cdot60}Fe_{0\cdot05}Ti_{0\cdot35})O_3$ annealed at 1100 °C for about 4 h.

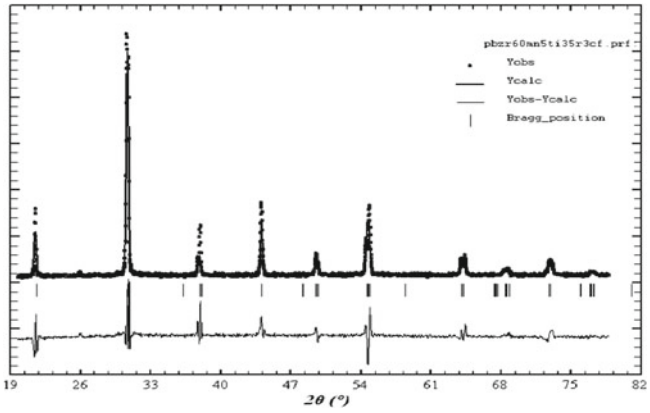

Figure 3. XRD pattern along with Rietveld refined data for sample $Pb(Zr_{0\cdot60}Mn_{0\cdot05}Ti_{0\cdot35})O_3$ annealed at 1100 °C. Pattern was refined using *R3c* space group with rhombohedral symmetry.

Table 1. Crystallite size and grain size of samples $Pb(Zr_{0\cdot65}Ti_{0\cdot35})O_3$, $Pb(Zr_{0\cdot60}Fe_{0\cdot05}Ti_{0\cdot35})O_3$ and $Pb(Zr_{0\cdot60}Mn_{0\cdot05}Ti_{0\cdot35})O_3$ annealed at different temperatures.

Sample composition	Crystallite size (nm)			Grain size (μm), SEM
	Scherrer's method	WH method	Rietveld method	
$Pb(Zr_{0\cdot65}Ti_{0\cdot35})O_3$ (900 °C)	16·8(3)	14·3(6)	13·5(7)	0·114(4)
$Pb(Zr_{0\cdot65}Ti_{0\cdot35})O_3$ (1100 °C)	34·6(4)	33·2(3)	33·0(9)	3·513(7)
$Pb(Zr_{0\cdot60}Fe_{0\cdot05}Ti_{0\cdot35})O_3$ (900 °C)	16·2(6)	14·1(3)	13·0(2)	0·111(9)
$Pb(Zr_{0\cdot60}Fe_{0\cdot05}Ti_{0\cdot35})O_3$ (1100 °C)	33·7(6)	32·9(3)	32·1(2)	3·423(5)
$Pb(Zr_{0\cdot60}Mn_{0\cdot05}Ti_{0\cdot35})O_3$ (900 °C)	15·9(6)	13·7(7)	12·5(7)	0·110(4)
$Pb(Zr_{0\cdot60}Mn_{0\cdot05}Ti_{0\cdot35})O_3$ (1100 °C)	32·5(3)	31·9(5)	30·1(7)	3·323(2)

where U, V and W are the usual peak shape parameters, IG the measure of isotropic size effect, D_{ST} the coefficient related to strain. IG and D_{ST} can be refined in Rietveld method. The crystallite size obtained from Rietveld refinement and grain size from SEM analysis is listed in table 1. The refined XRD patterns of $Pb(Zr_{0.60}Mn_{0.05}Ti_{0.35})O_3$ and $Pb(Zr_{0.60}Fe_{0.05}Ti_{0.35})O_3$ powders annealed at 1100 °C for 4 h are shown in figures 3 and 4, respectively. The experimental points are given as dot (•) and theoretical data are shown as solid line. Difference between theoretical and experimental data is shown as bottom line. The vertical line represents the Bragg's allowed peak. It is observed that all the observed peaks could be well refined. The lattice parameters and goodness of fit parameters are listed in table 2. The lattice parameters, occupancy, fractional atomic positions, etc were taken as free parameters during fitting. Here, we have refined eight parameters such as lattice parameters, occupancy, background, absorption coefficient, atomic positions, two theta zero error, thermal factors and profile peak functions. All the samples show that the crystal structure is rhombohedral with a space group $R3c$. The thermal effect and profile function refinement make fitting better than the other effect in refinement. Pseudo–Voigt description of profile shape was determined as a profile set up for Rietveld refinement. Refinement profile function value is used for modern commercial Bragg–Brentano diffractometer and value of the sample broadening. The lattice parameters and unit cell volumes decrease from Mn^{3+}–Fe^{3+} ion concentration and it could be due to the tolerance factor and larger ionic size of Mn^{3+} (0·66 Å) to that of Fe^{3+} (0·64 Å). The bond lengths and bond angles have been calculated for all the samples annealed at 1100 °C temperature as shown in table 2.

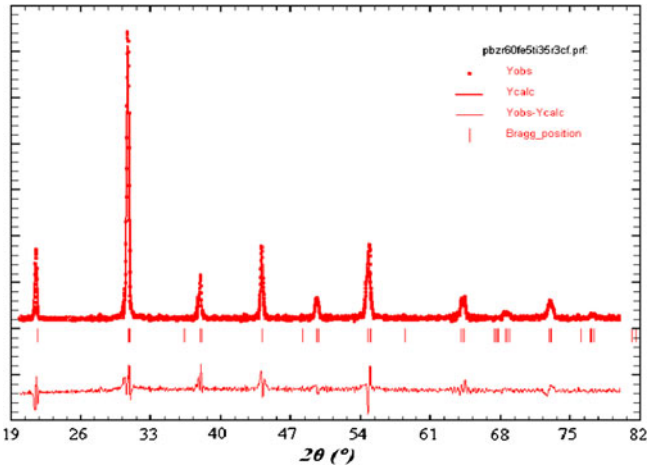

Figure 4. XRD pattern along with Rietveld refined data for sample $Pb(Zr_{0.60}Mn_{0.05}Ti_{0.35})O_3$ annealed at 1100 °C. Pattern was refined using $R3c$ space group with rhombohedral symmetry.

3.2 *Microstructural analysis*

Scanning electron microscope (SEM) is an useful technique to study the topography, morphology and composition of

Table 2. Microparameters obtained from Rietveld analysis of $Pb(Zr_{0.65}Ti_{0.35})O_3$, Pb $(Zr_{0.60}Mn_{0.05}Ti_{0.35})O_3$ and Pb $(Zr_{0.60}Fe_{0.05}Ti_{0.35})O_3$ samples annealed at 1100 °C for 4 h.

Sample → Parameters ↓	Pb $(Zr_{0.65}Ti_{0.35})O_3$	Mn = 0·05	Fe = 0·05
Space group	$R3c$	$R3c$	$R3c$
Pb (occup.)	0·9823(8)	0·9736(5)	0·9736(5)
Zr (occup.)	0·6443(2)	0·6013(5)	0·6013(5)
Ti (occup.)	0·3445(2)	0·3500(8)	0·3500(8)
Fe (occup.)	–	–	0·0543(6)
Mn (occup.)	–	0·0524(3)	–
O (occup.)	1·0000	1·0000	1·0000
$a = b$ (Å)	5·816(7)	5·812(2)	5·806(10)
c (Å)	14·1847(21)	14·127(6)	14·118(11)
Volume (Å^3)	415·65(10)	413·5501	413·1102
χ^2 (chi^2)	1·9	3·3	2·1
R_p	11·9	15·9	14·7
R_{wp}	11·5	14·2	13·6
R_{exp}	12·0	11·6	12·3
R_f	10·9	15·4	10·9
R_{Bragg}	10·1	11·7	11·9
∠Fe–Fe–Pb	–	–	70·80
∠Mn–Mn–Pb	–	70·30	–
∠Ti–Ti–Ti	–	83·43	80·36
Pb–Mn	–	0·74	–
Pb–Fe	–	–	0·73

the materials with much higher resolution. Scanning electron microscopy (SEM) of pure and substituted (Mn5% and Fe5%) samples on the B-site of compounds are shown in figure 5(a–c). From these micrographs, it is confirmed that the grains of different size are uniformly and densely distributed over the entire surface of the samples due to introduction of Mn^{3+} and Fe^{3+} ions, which are given in table 1. The shape, size and distribution of grains of the microstructure for all the samples were confirmed as polycrystalline in nature. For both Mn5% and Fe5%, doping grain size shows a decreasing trend with increase in Mn and Fe concentration. The reason for the decrease of both the crystallite and grain sizes can be attributed to segregation of Mn and Fe at grain boundaries (Dai *et al* 1995). The difference in structural parameters are because the crystallites are different from grains and XRD is a bulk study whereas SEM is a surface study. Therefore, XRD gives crystallite (particle) size and SEM gives grain size, which consists of crystallites.

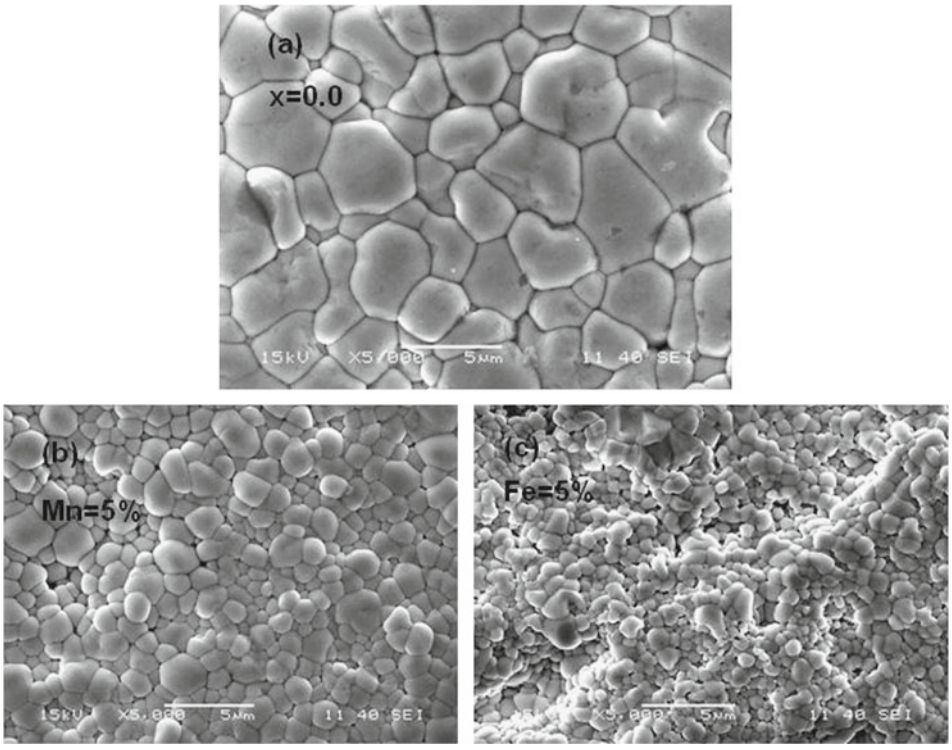

Figure 5. SEM micrographs for samples (**a**) $Pb(Zr_{0.65}Ti_{0.35})O_3$, (**b**) $Pb(Zr_{0.60}Mn_{0.05}Ti_{0.35})O_3$ and (**c**) $Pb(Zr_{0.60}Fe_{0.05}Ti_{0.35})O_3$ annealed at 1100 °C for 4 h.

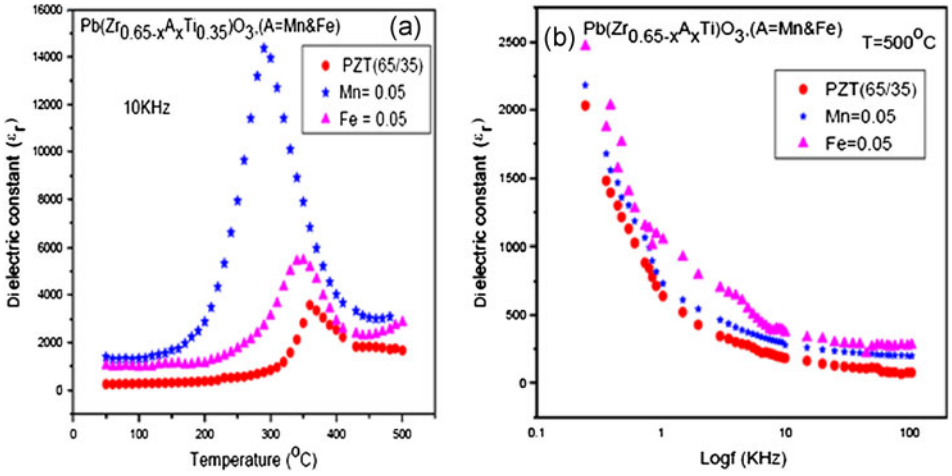

Figure 6. (**a**) Shows variation of dielectric constant with temperature at frequency 10 kHz and (**b**) shows variation of dielectric constant with log *f* at 500 °C temperature for samples $Pb(Zr_{0.65}Ti_{0.35})O_3$, $Pb(Zr_{0.60}Mn_{0.05}Ti_{0.35})O_3$ and $Pb(Zr_{0.60}Fe_{0.05}Ti_{0.35})O_3$.

3.3 *Dielectric analysis*

Figure 6(a) shows variation of dielectric constant vs temperature for pure and substituted samples on Zr site of the compound at a frequency, 10 kHz. It clearly indicates that dielectric constant increases gradually with increase in temperature for pure and doped samples on Zr site of the compound to its maximum value and then decreases, which confirms that a phase transition (from ferroelectric to paraelectric phase) occurs at a particular temperature, called as transition or Curie temperature (T_c) (Wilkinson *et al* 1994). On further increase in temperature, relative dielectric constant decreases for pure and substituted samples of the compound. The comparative dielectric data of pure and substituted samples at frequency, 10 kHz, are recapitulated in table 3. Here, T_c is maximum at pure sample and minimum for Mn-substituted sample. But one can observe that for pure PZT, the value of dielectric constant is less and T_c is more. For Mn doping, dielectric constant is more and T_c is less in comparison with Fe substitutions. This could be due to the different ionic radii and charge neutrality of the materials.

Table 3. Dielectric behaviours of pure and substituted samples (Mn and Fe) at 10 kHz.

Samples	ε_{max}	T_c (°C)
$Pb(Zr_{0.65}Ti_{0.35})O_3$	3549	363
$Pb(Zr_{0.60}Mn_{0.05}Ti_{0.35})O_3$	14245	292
$Pb(Zr_{0.60}Fe_{0.05}Ti_{0.35})O_3$	5432	346

Figure 6(b) shows value of dielectric constant decreasing with increase in frequency for pure and substituted samples at higher temperature (500 °C). This happens due to the presence of all types of polarizations (i.e. interfacial, ionic, dipolar, electronic and space charge) (Chua *et al* 2005; Ranjan *et al* 2009; Vijendra Chaudhari and Bichile 2010). At higher frequencies, the main contribution to dielectric constant comes from electronic polarization, as some of the polarizations become ineffective and thus, the value of dielectric constant decreases.

3.4 *A.C. conductivity analysis*

Figure 7(a–c) shows variation of a.c. conductivity vs inverse temperature of $Pb(Zr_{0.65}Ti_{0.35})O_3$, $Pb(Zr_{0.60}Mn_{0.05}Ti_{0.35})O_3$ and $Pb(Zr_{0.60}Fe_{0.05}Ti_{0.35})O_3$ ceramics at a frequency of 10 kHz. The a.c. conductivity ($\sigma_{a.c.}$) (Pradhan *et al* 2009; Tiwari and Choudhary 2009a, b), of the above ceramic materials can be calculated by using the relation

$$\sigma_{a.c.} = \omega \varepsilon_0 \varepsilon_r \tan\delta, \tag{4}$$

where $2\pi f = \omega$, ε_0 is the permittivity of free space, ε_r the relative dielectric constant, $\tan\delta$ the dissipation factor. The a.c. conductivity pattern indicates a progressive rise in conductivity with rise in temperature at a frequency of

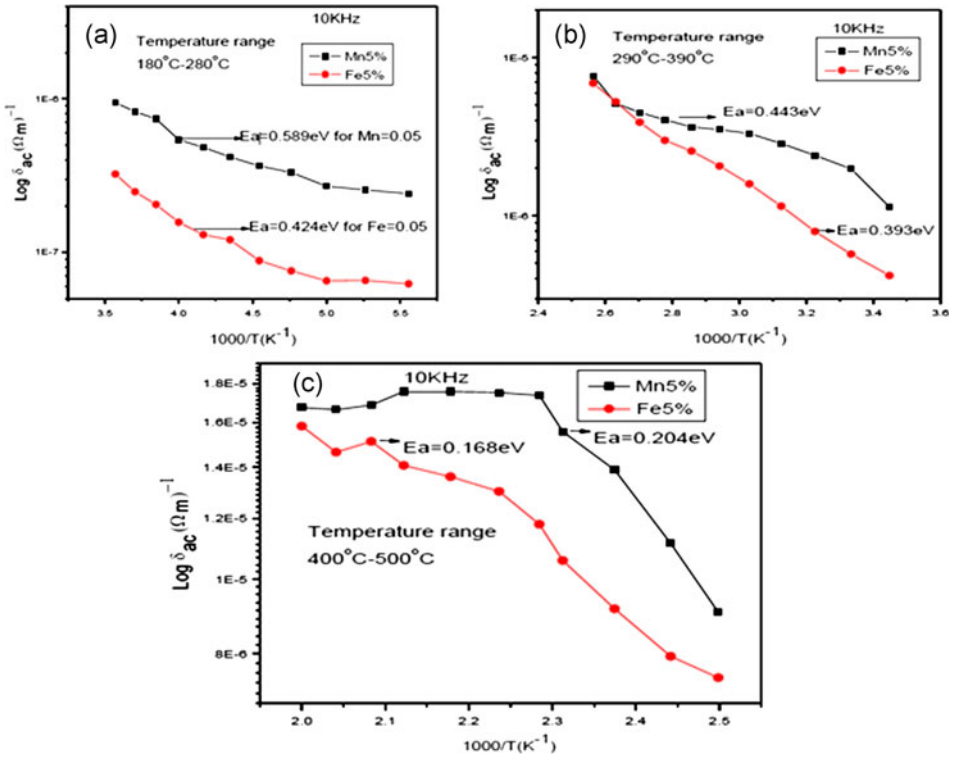

Figure 7. (**a–c**) Variation of log a.c. conductivity vs inverse of temperature at frequency, 10 kHz of samples $Pb(Zr_{0.60}Mn_{0.05}Ti_{0.35})O_3$ and $Pb(Zr_{0.60}Fe_{0.05}Ti_{0.35})O_3$.

Table 4. Activation energies of $Pb(Zr_{0.65-x}A_xTi_{0.35})O_3$, (A = Mn and Fe) at $x = 0.05$ samples at below and above transition temperature range at frequency 10 kHz in relation with a.c. conductivity plots.

Temperature range (°C)	Frequency (kHz)	Activation energy (eV)
180–280 (Mn = 0·05)	10	0·589
180–280 (Fe = 0·05)	10	0·424
290–390 (Mn = 0·05)	10	0·443
290–390 (Fe = 0·05)	10	0·393
400–500 (Mn = 0·05)	10	0·204
400–500 (Fe = 0·05)	10	0·168

10 kHz. A frequency independent relation between a.c. conductivity and temperature is studied as (Kumar and Yadav 2007; Shukla and Choudhary 2010)

$$\sigma = \sigma_0 \exp\left(\frac{-E_a}{k_B T}\right), \tag{5}$$

where σ_0 is a constant, k_B the Boltzmann constant and E_a the activation energy for conduction. The value of activation energy was found to be 0·589–0·424 eV for both the substitutions (5% of Mn and Fe). The activation energy decreases from Mn to Fe substitution in the low temperature region (ferroelectric region). The value of activation energy was found to be 0·443 for Mn and 0·393 eV for Fe in the paraelectric region (above transition temperature). Again for the temperature range 400–500 °C, the activation energy decreases with increase in temperature. All the activation energies are recapitulated in table 4 with different temperature ranges. This could be due to the smaller ionic radius and tolerance factor of Mn than Fe and it is in good agreement with earlier reported Pb-based polycrystalline ceramic materials and contains oxygen vacancies (Shukla *et al* 2010; Niranjan Sahu *et al* 2012). Finally, the value of activation energy decreases with increase in temperature for both Mn and Fe substitutions. The type of temperature dependent in a.c. conductivity indicates that the electrical conduction in the material is a thermally-activated process. It is well known that the motion of oxygen vacancies gives rise to activation energy of 1 eV in ceramic samples; usually oxygen vacancies are considered as one of the mobile charge carriers in perovskite ferroelectrics.

Figure 8 shows frequency variation of a.c. conductivity of a typical sample PZFT5 ($x = 0.05$). The a.c. conductivity data are fitted to the Jonscher's equation (Jonscher 1983; Macdonald 1987) and can be written as

$$\sigma_{a.c.} = A\omega^n. \tag{6}$$

Here, the fitting parameters A and n at various temperatures of a typical sample (PZFT5) ($x = 0.05$) is given in table 5. The frequency exponent, n is found to decrease with increase in temperature.

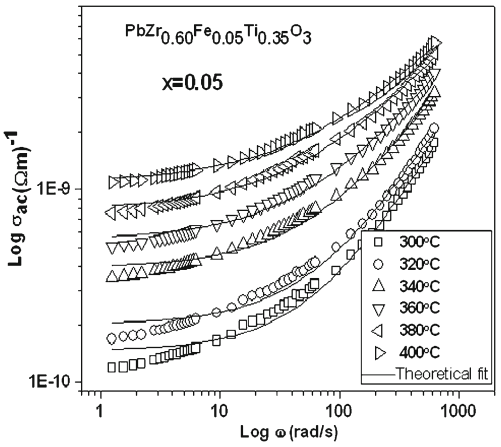

Figure 8. Variation of a.c. conductivity of sample $Pb(Zr_{0.65-x}Fe_xTi_{0.35})O_3 (x = 0.05)$ with frequency at different temperatures.

Table 5. Fitting parameters of a.c. conductivity from Jonscher's universal law of $Pb(Zr_{0.65-x}Fe_xTi_{0.35})O_3 (x = 0.05)$ ceramic.

Temperature (°C)	A	n
300	1.46×10^{-7}	0·997
320	2.04×10^{-7}	0·988
340	3.95×10^{-7}	0·890
360	5.54×10^{-7}	0·820
380	7.84×10^{-7}	0·743
400	1.09×10^{-6}	0·703

3.5 *Impedance analysis*

Electrical impedance or simply impedance, describes a measure of opposition to alternating current (a.c.). Electrical impedance extends the concept of resistance to a.c. circuits, describing not only the relative amplitudes of the voltage and current, but also the relative phases. When the circuit is driven with direct current (d.c.), there is no distinction between impedance and resistance; the latter can be thought of as impedance with zero phase angles. The symbol for impedance is usually z and it may be represented by writing its magnitude and phase in the form $z\angle\theta$. However, complex number representation is more powerful for circuit analysis purposes. The term impedance was coined by Oliver Heaviside (1886). Kennelly (1893) was the first to represent impedance with complex numbers in 1893. Impedance is defined as the frequency domain ratio of voltage to current. The magnitude of the complex impedance is the ratio of voltage to current amplitude.

Complex impedance spectrum (CIS) is a non-destructive and powerful experimental technique for the characterization of microstructural and electrical properties of some electronic materials over a wide range of frequency and temperature (Ivanova *et al* 1962). There are many ways by which CIS data may be plotted. In CIS field, where capacitive rather than inductive effects dominate, conventionally

one plots $\mathrm{Im}(Z) \cong -Z''$ on the y-axis vs $\mathrm{Re}(Z) \cong Z'$ on the x-axis to give a complex-plane impedance plot. Such graphs have been termed as Nyquist plots. But, it has the disadvantage of not indicating frequency response directly, but may nevertheless be very helpful in identifying conduction processes that all present. The complex impedance equations (Chaisan *et al* 2005) can be written as

$$Z^* = Z' - JZ'', \tag{7}$$

$$Z' = R/1 + (\omega RC)^2, \tag{8}$$

$$Z'' = R(\omega RC)/(1 + \omega RC)^2, \tag{9}$$

where Z' and Z'' are the real and imaginary components of impedance, ω the angular frequency, R and C are resistance and capacitance, respectively. $j^2 = -1$, this relation offers wide scope for a graphical analysis of the various parameters under different conditions of temperature or frequency. The systematic procedure for the analysis of a.c. measurements is to plot the results in the complex impedance plane; Z' vs Z''. These plots are useful for determining the dominant resistance of the sample. However, these are insensitive to smaller resistances. A separation of the grain and grain boundary properties has been achieved using an equivalent circuit model in impedance analysis. It is understood that at the peaks of semicircles, the equation (Adamczyk *et al* 2007) can be written as

$$2\pi f_{\max}\tau = 1, \tag{10}$$

here, τ is the mean relaxation time. The Nyquist plots of both doped and pure samples at different temperatures are shown in figure 9(a–c) (300–360 °C). The high-frequency curve attributes to the bulk properties of the material and arises due to parallel combination of the bulk resistance (R_g) and bulk capacitance (C_g), whereas the low frequency semicircles are attributed to the grain boundary effects. The semicircles at high frequency correspond to the bulk response, which is commonly observed in other ceramic materials (Sinclair and East 1989; Bahuguna *et al* 2003). Nyquist plot compares the complex impedance plots (symbols) with theoretically fitted data (solid line) using commercially available software ZSIMP WIN Version 2. The electrical equivalent circuit corresponding to the sample impedance response is shown as an inset in figure 9(a–c). An equivalent circuit is commonly used in impedance spectroscopy analysis to provide a complete picture of the system and establish the structure–property relationship of the materials. This plays an important role in the interpretation of electrical behaviour of the material. The observed values of grain capacitance (C_g), grain resistance (R_g) and apparent bulk conductivity (σ_b) of all the samples at different temperatures are given in

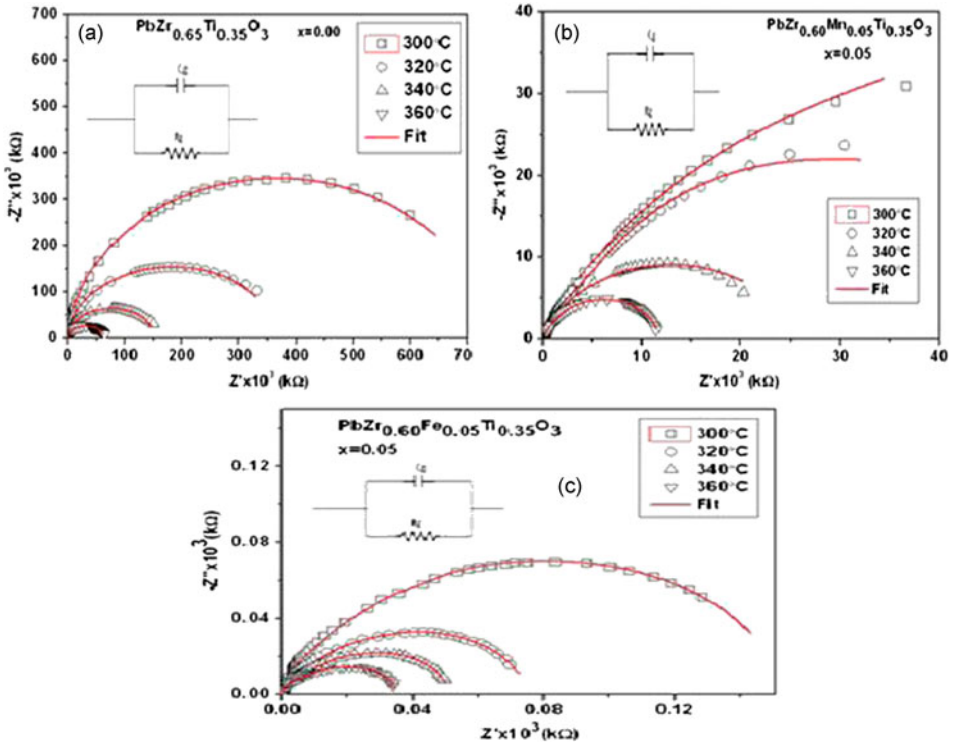

Figure 9. (**a–c**) Shows Nyquist plot of $Pb(Zr_{0.65}Ti_{0.35})O_3$, $Pb(Zr_{0.60}Mn_{0.05}Ti_{0.35})O_3$ and $Pb(Zr_{0.60}Fe_{0.05}Ti_{0.35})O_3$ at different temperatures (300–360 °C) with scattered points showing experimental data and solid line showing fitting data.

Table 6. Observed value of grain capacitance (C_g), grain resistance (R_g) and apparent bulk conductivity (σ_b) of $Pb(Zr_{0.65-x}A_xTi_{0.35})O_3$(A = Mn and Fe) at $x = 0.05$ samples at different temperatures.

Sample	Temperature (°C)	C_g (nF)	R_g (kΩ)	$\sigma_b = t/R_gA$ $(\Omega m)^{-1}$
$x = 0.00$	300	3·640	7.36×10^5	2.348×10^{-7}
	320	2·530	2.981×10^5	5.80×10^{-7}
	340	2·186	1.263×10^5	1.369×10^{-6}
	360	1·791	5.425×10^4	3.188×10^{-6}
Mn = 0·05	300	2·401	1.215×10^3	1.50×10^{-6}
	320	2·371	2.146×10^4	8.54×10^{-6}
	340	2·284	4.457×10^4	4.11×10^{-6}
	360	2·231	7.251×10^3	2.52×10^{-5}
Fe = 0·05	300	1·446	6.05×10^5	3.09×10^{-7}
	320	1·349	3.34×10^4	5.584×10^{-6}
	340	1·261	2.35×10^4	7.94×10^{-6}
	360	1·210	1.61×10^4	1.15×10^{-5}

table 6. It has been observed that sample resistance decreases with an increase in temperature, which is an effective analogous to the negative temperature coefficient of resistance (NTCR) in the conventional semiconductors. So, the result indicates a typical semiconducting behaviour of the materials. D.C. conductivity is calculated from the grain resistance, R_g, using the formula

$$\sigma_{d.c.} = t/R_gA, \tag{11}$$

here t is the thickness of the sample and A the area of the electrode deposited on the sample. From the value of relaxation time, it can be said that it is a temperature-dependent phenomena.

4. Conclusions

Polycrystalline sample of $Pb(Zr_{0.65-x}A_xTi_{0.35})O_3$ (A = Mn and Fe) ($x = 0.00, 0.05$) perovskite ceramics have been prepared by conventional solid-state reaction technique. All the samples are in single-phase form with rhombohedral structure and having a space group $R3c$. The substitution of Mn and Fe (both 5%) at the Zr-site of PZT does not provide any change in its crystal structure, but it changes the particle density on the surface. Microstructural analysis of the surface of the compounds by scanning electron microscopy (SEM) suggests that there is a significant change in grain size and density due to introduction of Mn and Fe on B-site of the compounds. Ferroelectric to paraelectric phase transition occurs for all the samples. From conductivity analysis, we observed that the value of activation energy decreases with increase in temperature for both Mn and Fe substitutions. The activation energy of the materials was found sensitive to its crystallite size due to oxygen vacancies, responsible for conduction mechanism. Both the modified samples are obeying Jonscher power law. From Nyquist plots, grain resistance of the material decreases with rise in temperatures showing negative temperature coefficient of resistance which indicates semiconducting behaviour of the materials.

Acknowledgements

We are grateful to Dr A K Thakur, Department of Physics and Meteorology, Indian Institute of Technology, Kharagpur, for his useful suggestions and extending laboratory facilities for dielectric measurements.

References

Adamczyk M, Ujma Z, Szymczak L, Soszynski A and Koperski J 2007 *Mater. Sci. Eng.* **B136** 170
Ang C, Yu Z and Cross L E 2000 *Phys. Rev.* **B62** 228
Bahuguna B V, Saradhi, Srinivas K, Prasad G, Suryanarayana S V and Bhimasankaram T 2003 *Mat. Sci. Eng.* **B98** 10
Behera B, Nayak P and Choudhary R N P 2007 *Phys. Status Solidi* **204** 2479
Boucher E, Guyomar D, Lebrun L, Guiffard B and Grange G 2002 *J. Appl. Phys.* **92** 5437
Chaisan W, Yimnirun R, Ananta S and Cann D P 2005 *Mater. Lett.* **59** 3732
Chua B W, Lu L, Lai M O and Wong G H L 2005 *J. Alloys Compd.* **386** 303
Dai X, Xu Z and Viehland D 1995 *J. Am. Ceram. Soc.* **7810** 2815
Dimza V I 1996 *J. Phys. Condens. Matter* **8** 2887
Dorr K 2006 *J. Phys. D (Berlin)* **39** R125
Dutta S, Choudhary R N P, Sinha P K and Thakur A K 2004 *J. Appl. Phys.* **96** 1607
Haertling G H, in Buchanan R C (ed.) 1991 *J. Ceram. Mater. Elect.* (New York: Marcel Dekker) Ch. 3
Härdtl K H and Hennings D 1972 *J. Am. Ceram. Soc.* **55** 230
Herbert J M 1985 *Ferroelectric transducers and sensors* (London: Gordon and Breach Science Publishers) p. 299
Ivanova V V, Kapyshev A G, Venevtsev Yu N and Zhadanov G S 1962 *Izv. ANSSSR, Ser. Fiz.* **26** 354

Jaffe B, Crook W R and Jaffe H 1971 *Piezoelectric ceramics* (New York: Academic Press)
Jin B M and Kim J S C 1997 *Appl. Phys.* **A65** 53
Jonscher A K 1983 *Dielectric relaxation in solids* (London: Chelsa Dielectrics)
Kennelly Arthur 1893 *Impedance (IEEE)*
Klung H P and Alexander L B 1974 *X-ray diffraction procedures* (New York: Wiley) p. 687
Kumar M and Yadav K L 2007 *J. Phys. Condens. Matter* **19** 242
Lines M E and Glass A M 1977 *Principles and Applications of Ferroelectric and Related Materials* (Oxford: Clarendon Press) p. 294
Macdonald J R 1987 *Impedance spectroscopy* (New York: Wiley)
Maiti T, Guo R and Bhalla A S 2007 *Appl. Phys. Lett.* **90** 182901
Majumder B, Roy B, Krupanidhi S B and Katiyar R S 2001 *Appl. Phys. Lett.* **79** 239
Niranjan Sahu and Panigrahi S 2012 *Ceram. Int.* **38** 1085
Niranjan Sahu, Panigrahi S and Manoranjan Kar 2011 *J. Adv. Powd. Technol.* **22** 689
Niranjan Sahu, Panigrahi S and Manoranjan Kar 2012 *Ceram. Int.* **38** 1549
Oliver Heaviside 1886 *The Electrician*, p. 212, 23rd July 1886, reprinted as Electrical Papers, p. 64, AMS Bookstore, ISBN 0821834657
Pandey S K, Thakur O P, Bhattacharya D K, Prakash C and Chatterjee R 2009 *J. Alloys Compd.* **468** 356
Pradhan D K, Choudhary R N P, Rinaldi C and Katiyar R S 2009 *J. Appl. Phys.* **106** 024102
Rangaraju M R and Choudhary R N P 2004 *J. Mater. Sci.* **39** 1765
Ranjan R, Kumar Kalyani A, Garg R and Krishna P S R 2009 *Solid State Commun.* **149** 2098
Rukmini H R 1998 *Structural and electrical properties of sol-gel derived La (Li, K, Na) modified PLZT ceramics*. Ph.D. Thesis, Indian Institute of Technology, Kharagpur, p. 71
Rukmini H R, Choudhary R N P and Prabhakara D L 2000 *Mater. Chem. Phys.* **64** 171
Saha S and Krupanidhi S B 2000 *J. Appl. Phys.* **87** 849
Saha S and Sinha T P 2006 *J. Appl. Phys.* **99** 014109
Shukla A and Choudhary R N P 2010 *Physica* **B405** 2508
Sinclair D C and East J 1989 *J. Appl. Phys.* **66** 3580
Tanasoiu C, Dimitriu E and Miclea C 1999 *J. Eur. Ceram. Soc.* **19** 1187
Taylor A 1961 *X-ray metallography* (New York: Wiley)
Teguh Yogaraksa, Muhammad Hikam and Irzaman 2004 *Ceram. Int.* **30** 1483
Thakur O P, Prakash C and James A R 2009 *J. Alloys Compd.* **470** 548
Tiwari B and Choudhary R N P 2008 *AIP conference proceeding/Materials Physics and Applications*, ISBN: 9780735405936, Innbundet
Tiwari B and Choudhary R N P 2009a *Solid State Sci.* **11** 219
Tiwari B and Choudhary R N P 2009b *Physica* **B404** 4111
Vijendra Chaudhari A and Bichile G K 2010 *Physica* **B405** 534
Wilkinson A P, Speck J S, Cheetham A K, Natarajan S and Thomas J M 1994 *J. Chem. Mater.* **6** 750
Williamson G K and Hall W H 1953 *Acta Met.* **1** 22
Xu J, Gao C, Zhai J, Yao X, Xue J and Huang Z 2006 *J. Cryst. Growth* **291** 130
Young R A 1996 *The Rietveld method* in *International Union of Crystallography* (New York: Oxford University Press)